Hydrogen Evolution

Deutsche Ausgabe: DOI: 10.1002/ange.201600431
Internationale Ausgabe: DOI: 10.1002/anie.201600431

Hierarchical Integration of Photosensitizing Metal–Organic Frameworks and Nickel-Containing Polyoxometalates for Efficient Visible-Light-Driven Hydrogen Evolution

*Xiang-Jian Kong, Zekai Lin, Zhi-Ming Zhang, Teng Zhang, and Wenbin Lin**

Abstract: *Metal–organic frameworks (MOFs) provide a tunable platform for hierarchically integrating multiple components to effect synergistic functions that cannot be achieved in solution. Here we report the encapsulation of a Ni-containing polyoxometalate (POM) $[Ni_4(H_2O)_2(PW_9O_{34})_2]^{10-}$ (**Ni_4P_2**) into two highly stable and porous phosphorescent MOFs. The proximity of **Ni_4P_2** to multiple photosensitizers in **Ni_4P_2**@MOF allows for facile multi-electron transfer to enable efficient visible-light-driven hydrogen evolution reaction (HER) with turnover numbers as high as 1476. Photophysical and electrochemical studies established the oxidative quenching of the excited photosensitizer by **Ni_4P_2** as the initiating step of HER and explained the drastic catalytic activity difference of the two POM@MOFs. Our work shows that POM@MOF assemblies not only provide a tunable platform for designing highly effective photocatalytic HER catalysts but also facilitate detailed mechanistic understanding of HER processes.*

Metal–organic frameworks (MOFs) have attracted considerable attention for their unprecedentedly high surface areas and well-defined pore structures that can be readily tuned via judicious selection of bridging ligands and metal-connecting nodes.[1,2] In particular, potential applications of MOFs in gas storage and separations have been extensively studied in the past decade.[2,3] By introducing catalytically competent moieties via either the bridging ligands or the metal-connecting nodes, MOFs have also emerged as a new class of recyclable and reusable single-site solid catalysts for a broad range of organic transformations.[4,5] Encapsulation of metal and metal-oxide (such as Au, Pd, Pt, ZnO) nanoparticles in MOF cavities has recently been demonstrated to be another effective strategy for preparing heterogeneous catalysts with high activities.[6,7]

Photocatalytic hydrogen evolution reaction (HER) is an essential half reaction of water splitting,[8,9] in which effective generation of charge-separated excited states (electron-hole pairs) is followed by facile transfer of the electrons to HER centers to reduce proton to hydrogen.[10] Recent studies have shown the feasibility of integrating the two essential components—the photosensitizer and the HER catalyst—into MOFs to enable light-driven proton reduction.[11–13] For example, by loading noble metal Pt nanoparticles into the cavities of a photosensitizing MOF, we showed that the Pt@MOF system facilitated electron injection from the MOF framework to the encapsulated Pt nanoparticles to enable photocatalytic proton reduction with a high turnover number of ca. 7000.[13]

As a large family of nano-sized inorganic clusters with oxygen-rich surfaces, polyoxometalates (POMs) can readily undergo multi-electron reduction and oxidation processes, thus representing excellent candidates as HER and water oxidation catalysts.[14,15] In order to transition to HER catalysts based on earth-abundant elements, we recently used the noble-metal-free Wells-Dawson POM $[P_2W_{18}O_{62}]^{6-}$ as the electron acceptor to construct the POM@MOF molecular catalytic system for photocatalytic HER.[15] The $[P_2W_{18}O_{62}]$@MOF system enabled visible-light-driven HER as a result of fast six-electron injection from multiple $[Ru(bpy)_3]^{2+}$ ligands to each encapsulated $[P_2W_{18}O_{62}]^{6-}$ cluster, but at a modest TON of 79. In this system, methanol functions as a sacrificial donor, which is interesting with few literature precedents.[16] Transition-metal-substituted POMs have recently been shown to possess higher visible-light photocatalytic activity, because of their extensive tunability, rich redox chemistry, and synergism between the heterometallic ions.[17,18] Herein we report the design of a highly effective photocatalytic HER system by encapsulating Ni-containing POM $[Ni_4(H_2O)_2(PW_9O_{34})_2]^{10-}$ (**Ni_4P_2**) into $[Ir(ppy)_2(bpy)]^+$-derived UiO-MOF (ppy is 2-phenylpyridine and bpy is 2,2′-bipyridine). We also carried out detailed photophysical and electrochemical studies to establish the HER mechanism and to account for the catalytic activity difference between two different **Ni_4P_2**@MOFs.

The $[Ir(ppy)_2(bpy)]^+$-derived dicarboxylic acid (H_2**L_1**) or $[Ru(bpy)_3]^{2+}$-derived dicarboxylic acid (H_2**L_2**) was synthesized as reported previously.[12,15] MOF-**1**, formulated as $[Zr_6(\mu_3\text{-}O)_4(\mu_3\text{-}OH)_4(\mathbf{L_1})_6]\cdot(CF_3CO_2)_6$, and MOF-**2**, formulated as $[Zr_6(\mu_3\text{-}O)_4(\mu_3\text{-}OH)_4(\mathbf{L_2})_6]\cdot(CF_3CO_2)_{12}$, were obtained by treating $ZrCl_4$ and H_2**L_1**/H_2**L_2** in DMF at 100 °C for 72 h. **Ni_4P_2**@MOF-**1** (**1a**–**1f**) and **Ni_4P_2**@MOF-**2** (**2a**–**2f**) were prepared via in situ assembly by heating a mixture of $ZrCl_4$, H_2**L_1**/H_2**L_2** and **Ni_4P_2** at different molar ratios. Powder X-ray diffraction (PXRD) studies show that both MOF-**1** and MOF-**2** adopt UiO structures with large tetrahedral and octahedral cavities (Figure 1).[19] Based on charge balance, six and twelve

[*] Dr. X. J. Kong, Z. Lin, Dr. Z. M. Zhang, T. Zhang, Prof. W. Lin
Department of Chemistry, University of Chicago
929 E. 57th Street, Chicago, IL 60637 (USA)
E-mail: wenbinlin@uchicago.edu
Dr. X. J. Kong, Dr. Z. M. Zhang, Prof. W. Lin
Collaborative Innovation Center of Chemistry for Energy Materials, Department of Chemistry, College of Chemistry and Chemical Engineering, Xiamen University
Xiamen 361005 (P.R. China)

Supporting information for this article can be found under: http://dx.doi.org/10.1002/anie.201600431.

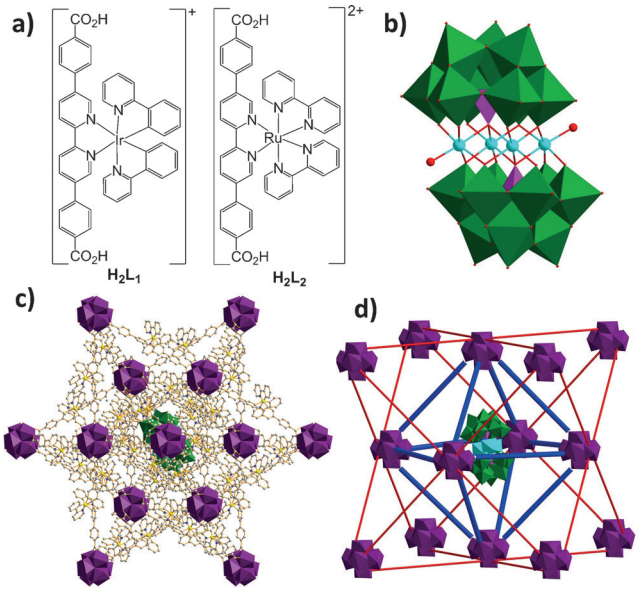

Figure 1. a) Chemical structures of H_2L_1 and H_2L_2. b) Polyhedral view of the structure of $[Ni_4(H_2O)_2(PW_9O_{34})_2]^{10-}$ (**Ni_4P_2**). c) Structural model of **Ni_4P_2**@MOF as viewed along the [1,1,1] direction. d) Structural model showing unoccupied tetrahedral cavities and the central **Ni_4P_2**-loaded octahedral cavity.

$CF_3CO_2^-$ anions per molecular formula are present in the cavities of MOF-**1** and MOF-**2**, respectively. The large cationic polyhedral cavities in the UiO structures are ideally suited for the encapsulation of the anionic **Ni_4P_2** POM. As the **Ni_4P_2** loading increased, the strong diffraction peaks at $2\theta = 3.96$ and 7.92° became weaker while the weak diffraction peaks at $2\theta = 4.56$, 6.56 and 7.56° became stronger in **1a–1f** (Figure 2). A similar trend was also observed for **2a–2f**. Since the tetrahedral cage of 1.4 nm is smaller than the large dimension of the **Ni_4P_2** POM (1.6 nm), only octahedral cages (2.2 nm) can encapsulate **Ni_4P_2** POMs (Figure S3 in the Supporting Information). The selective encapsulation in octahedral cages is supported by the similarity between the observed and simulated PXRDs of the POM@MOF (Figure 2a).

The loadings of **Ni_4P_2** in **Ni_4P_2**@MOF-**1** and **Ni_4P_2**@MOF-**2** were quantified by inductively coupled plasma-mass spectrometry (ICP-MS). The **Ni_4P_2** loadings were in the range of 0.005–0.34 for **1a–1f** and 0.008–0.53 for **2a–2f** per molecular formula (calculated based on the ratio of W_{18}/Zr_6, Table S3). Thermogravimetric analysis results for **1a–1f** and **2a–2f** (Figures S6 and S7) were consistent with these loadings. The stability of **Ni_4P_2** during the POM@MOF synthesis was supported by electrospray ionization-mass spectrometry (ESI-MS) (Figure S4). The observed peaks are consistent with the calculated mass for POM-related species (Table S4), suggesting the chemical stability of **Ni_4P_2** during **Ni_4P_2**@MOF synthesis.

The integration of the photosensitizing MOF framework and the POM catalyst allows for facile electron transfer to enable photocatalytic proton reduction. The visible-light-driven ($\lambda > 400$ nm) HER catalytic activities of **Ni_4P_2**@MOFs were studied in an acidic aqueous solution (pH 1.2) with methanol as the sacrificial electron donor. The amounts of H_2 generated were quantified by gas chromatography analysis of the headspace gas in the reactor. H_2 production increased linearly with time at a rate of 4.4 mmol h^{-1} g^{-1} with respect to $[Ni_4(H_2O)_2(PW_9O_{34})_2]^{10-}$ for **1a** (Figure 2c). The turnover number (TON) [defined as $n(1/2H_2)$] reached 1476 in 72 h irradiation. The HER TON of **1a–1d** inversely depended on the **Ni_4P_2** loading in the POM@MOF, which is consistent with the need of injecting multiple electrons in the HER process (Figure S8).

The **Ni_4P_2**@MOF-**1** catalyst was recovered and used for photocatalytic HER for three times with only a slight decrease of TON (346 ± 53, 329 ± 77, 297 ± 65; Figure S9). ICP-MS studies showed that only 0.2% Ir leached into the solution after 20 h photocatalytic HER. Transmission electron microscope (TEM) images of **Ni_4P_2**@MOF-**1** remained unchanged before and after photocatalysis (Figure S10), whereas PXRD patterns of the solid recovered after 20 h reactions were similar to those of the pristine **Ni_4P_2**@MOF-**1** catalyst (Figure 2d). We also performed elemental mapping and EDX studies of POM elements of **Ni_4P_2**@MOF before and after photocatalytic experiments. As shown in Figure S11–S13, the W, Ni, P elements are uniformly distributed throughout the microcrystals, suggesting the stability of **Ni_4P_2** during the POMOF synthesis and the photocatalytic HER reaction. **Ni_4P_2**@MOFs before and after photocatalytic experiments were digested and analysed with ESI-MS to confirm the stability of **Ni_4P_2** (Table S4–S5, Figure S4–S5). Control experiments using MOF-**1** without encapsulated **Ni_4P_2** and homogeneous mixtures of $[Ni_4(H_2O)_2(PW_9O_{34})_2]^{10-}$ and Me_2L_1 produced only trace amounts of H_2 (with TONs < 13 and 2) after 20 h of visible-light irradiations. These results indicate that the **Ni_4P_2**@MOF-**1** catalyst is stable and the hierarchical organization of the photosensitizing framework and the **Ni_4P_2** POM in **Ni_4P_2**@MOF-**1** is responsible for the high photocatalytic HER. The actinometric measurement with 460 nm light irradiation showed that **1a** has a modest quantum efficiency (QE) of 2×10^{-5}.

The $[Ru(bpy)_3]^{2+}$-derived **Ni_4P_2**@MOF **2a–2d** were also used in photocatalytic H_2 production experiments. To our surprise, **2a–2e** only gave trace amounts of H_2 after 20 h visible-light irradiations under the same photocatalytic conditions as **1a** (Table S6). The HER TONs are ≤ 3 for **2a** and ≤ 1 for **2b–2e**. This background-level TON values indicates that the $[Ru(bpy)_3]^{2+}$-derived **Ni_4P_2**@MOF-**2** are inactive for photocatalytic HER.

To investigate the HER mechanism, we studied electron transfer processes by luminescence quenching and lifetime measurements. The photosensitizer excited state can be quenched either reductively (by the methanol electron donor) or oxidatively (by the **Ni_4P_2** electron acceptor), which can be ascertained by measuring the luminescence of Me_2L_1 and Me_2L_2 with added methanol or **Ni_4P_2**. As shown in Figure 3c and 3d, the luminescence of Me_2L_1 was efficiently quenched by **Ni_4P_2** but was not affected much by the added methanol, suggesting that the first step of photocatalytic HER mainly occurs via electron transfer from the photosensitizer excited state to **Ni_4P_2** (i.e., oxidative quenching) but not via electron transfer from methanol to the photo-generated

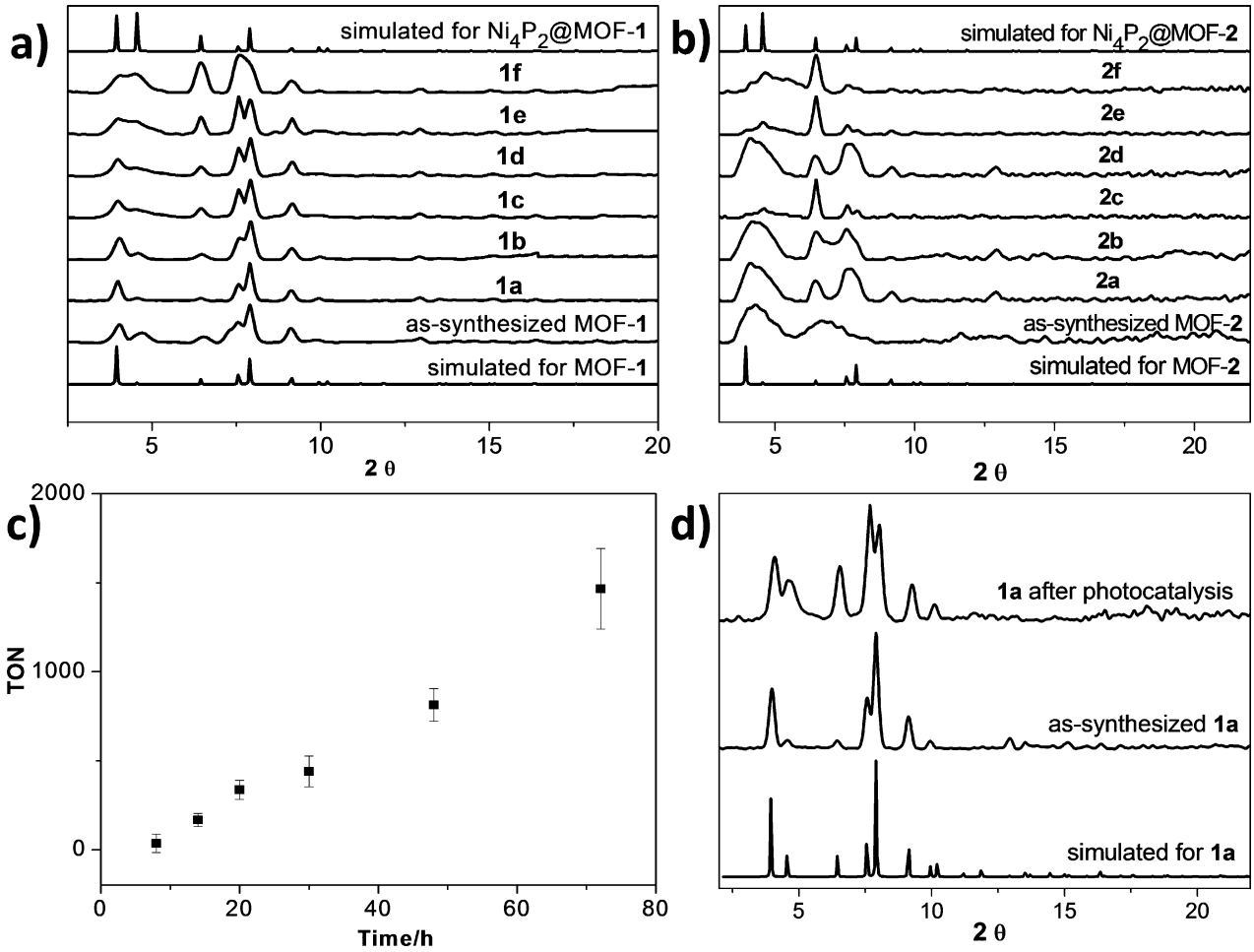

Figure 2. a) Predicted and experimental PXRD patterns of MOF-**1** and Ni_4P_2@MOF-**1** (**1a–1f**). b) Predicted and experimental PXRD patterns of MOF-**2** and Ni_4P_2@MOF-**2** (**2a–2f**). c) Time-dependent TONs of **1a** with methanol as the sacrificial electron donor in aqueous solution (pH 1.2) under visible-light ($\lambda > 400$ nm) irradiations. d) PXRD of **1a** before and after photocatalytic reaction.

electron-hole pair of the photosensitizer (i.e., reductive quenching). This oxidative quenching mechanism is further supported by time-resolved photoluminescence measurements of MOF-**1**, **1a–1f**, MOF-**2**, and **2a–2f**. As shown in Table S8, MOF-**1** exhibited a lifetime of 201 ns upon excitation at 405 nm, consistent with the long-lived ^{3}MLCT phosphorescence emission. The lifetimes are 154, 166, 166, 142,133, and 74.8 ns for **1a–1f**. Lifetimes of the ligand $Me_2\mathbf{L_1}$ and homogeneous solutions of $Me_2\mathbf{L_1}$ and $\mathbf{Ni_4P_2}$ are 77.9, 77.8, 77.6, 76.9, 75.4, 68.9 and 59.4 ns, respectively. Comparisons of lifetime decreases of $\mathbf{Ni_4P_2}$@MOFs and corresponding homogeneous solutions caused by the quencher indicate that $\mathbf{Ni_4P_2}$@MOF exhibited enhanced quenching, which can be attribute to the facile electron transfer from the excited photosensitizer to the POM due to their proximity to each other.

Cyclic voltammograms (CVs) of the photosensitizer and $\mathbf{Ni_4P_2}$ were studied to provide additional insights into the H_2 production mechanism. $\mathbf{Ni_4P_2}$ shows two reversible reduction peaks at −0.37 and −0.55 V vs. NHE and an irreversible catalytic peak with an onset potential of −0.65 V (Figure 4), suggesting that the H_2 production commences upon the injection of three electrons. This is supported by differential pulse voltammetry which showed a proton reduction peak at −0.66 eV for $\mathbf{Ni_4P_2}$ (Figure 4b). Based on these experimental data, we propose the photocatalytic HER mechanism in Scheme 1 for $\mathbf{Ni_4P_2}$@MOF-**1**. Under the visible-light irradiation, the ligand $[Ir(ppy)_2(bpy)]^+$ will be excited to the $[Ir(ppy)_2(bpy)]^{+*}$ excited state, which can transfer one

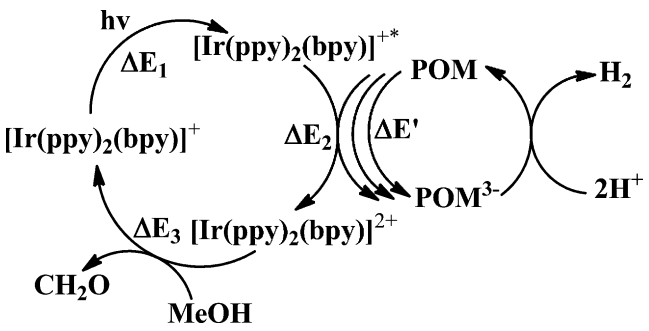

Scheme 1. Proposed catalytic cycle for visible-light-driven hydrogen evolution catalyzed by $\mathbf{Ni_4P_2}$@MOF-**1**.

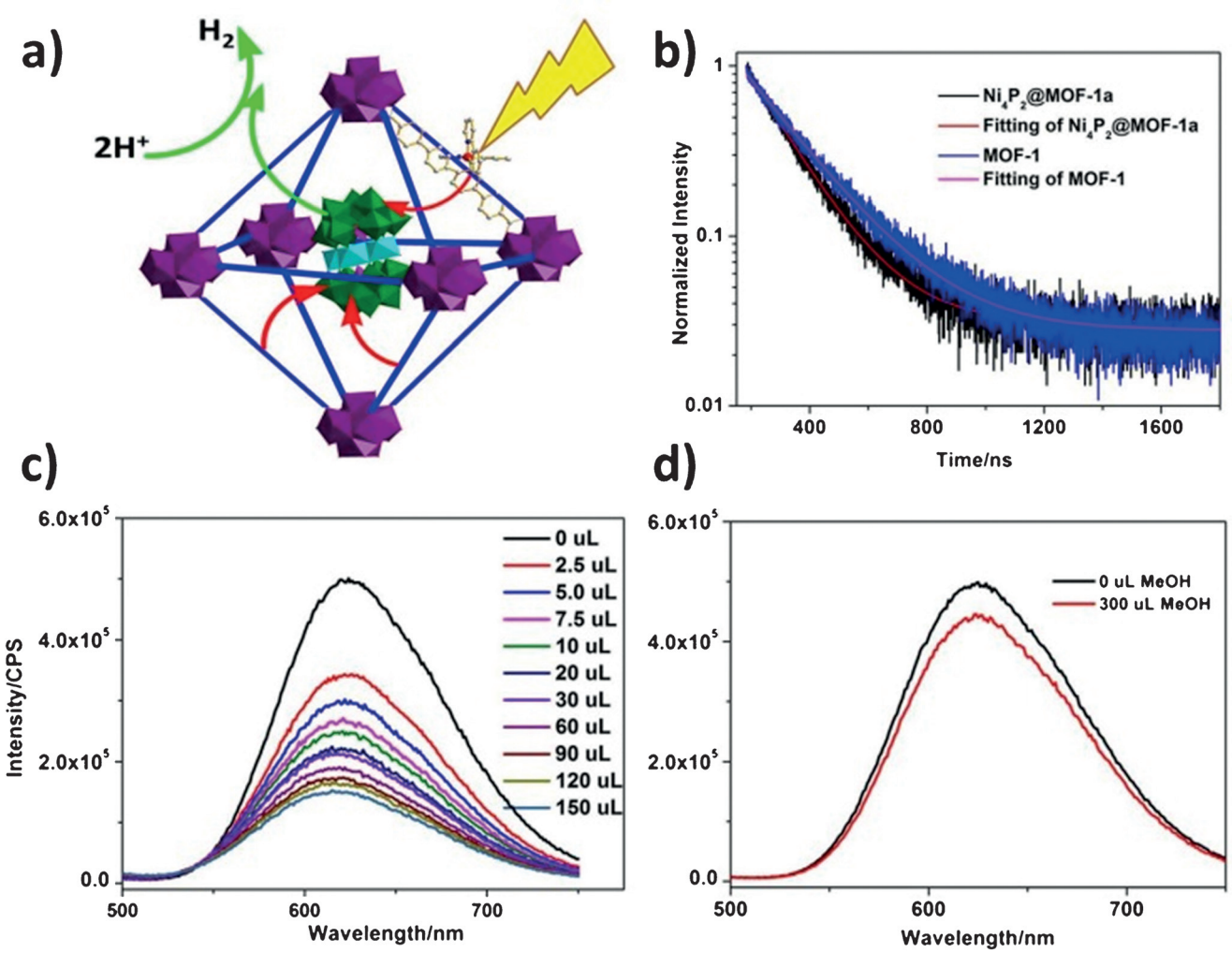

Figure 3. a) Schematic showing the injection of three electrons to the same $\mathbf{Ni_4P_2}$ upon photoexcitation of the MOF framework to enable proton reduction. b) Normalized luminescence decay trace of Ni_4P_2@MOF-**1a** and MOF-**1** measured at the 625 nm emission wavelength (with 405 nm excitation) in CH_3CN; the emission decays were fit to exponential expression $A = A_0 + A_1 e^{-t/\tau 1}$. The fitted curve is marked in red. c,d) Emission spectra of $\mathbf{Me_2L_1}$ (0.05 mM) after the addition of different amounts of $\mathbf{Ni_4P_2}$ (c) and 300 μL MeOH (d) in CH_3CN with 405 nm excitation.

electron to the $\mathbf{Ni_4P_2}$ POM to generate $[Ir(ppy)_2(bpy)]^{2+}$. After each POM has accepted three electrons, the $[POM]^{3-}$ can drive the proton reduction to generate H_2. The $[Ir(ppy)(bpy)]^{2+}$ can be reduced back to the $[Ir(ppy)(bpy)]^{+}$ by the MeOH sacrificial donor to complete the catalytic cycle. We quantified the amount of formaldehyde formed from the oxidation of methanol by gas chromatography-mass spectrometry (GC-MS).[20] After 20 hours of visible-light irradiation, the POM@MOF-**1a** produced 0.27 umol of formaldehyde, which is consistent with the expected value of 0.24 umol.

CV scans showed that $\mathbf{Me_2L_1}$ and $\mathbf{Me_2L_2}$ displayed oxidation peaks at 1.38 and 1.34 eV, respectively (Figure 4c). As shown in Figure 4d, $\mathbf{Me_2L_1}$ and $\mathbf{Me_2L_2}$ exhibits luminescence emission peaks at 598 nm and 633 nm, respectively. These correspond to energy gaps between the photosensitizer excited state and ground state of 2.08 and 1.96 eV for $\mathbf{Me_2L_1}$ and $\mathbf{Me_2L_2}$, respectively. Based on the energy loop as shown in Scheme 1, the energy difference $\Delta E'$ between $[Ir(ppy)_2(bpy')]^{+*}$ and $[Ir(ppy)_2(bpy)]^{2+}$ is 1.38–2.08 = −0.70 eV, which is negative enough (compared to −0.65 eV for proton reduction by $\mathbf{Ni_4P_2}$) to drive the H_2 production. In contrast, the energy gap $\Delta E'$ between $[Ru(bpy)_2(bpy')]^{2+*}$ and $[Ru(bpy)_2(bpy')]^{3+}$ is 1.34–1.96 = −0.62 eV, which is not negative enough to drive H_2 production by $\mathbf{Ni_4P_2}$. This analysis thus explains why **2a**–**2f** are inactive for photocatalytic HER with methanol as the sacrificial electron donor.

In summary, we have successfully encapsulated tetranickel-containing $\mathbf{Ni_4P_2}$ POMs into the pores of phosphorescent MOFs built from $[Ir(ppy)_2(bpy)]^{+}$ and $[Ru(bpy)_3]^{2+}$-derived dicarboxylate ligands. Visible-light-driven hydrogen evolution experiments show that the proximity of $\mathbf{Ni_4P_2}$ to multiple photosensitizers in $\mathbf{Ni_4P_2}$@MOF is key to facile multi-electron transfer and efficient HER. Photophysical and electrochemical studies established the oxidative quenching of the photosensitizer excited state by $\mathbf{Ni_4P_2}$ as the initiating step of HER and explained the drastic catalytic activity difference between the two POM@MOF systems. Hierarchically organized POM@MOF assemblies thus not only provide

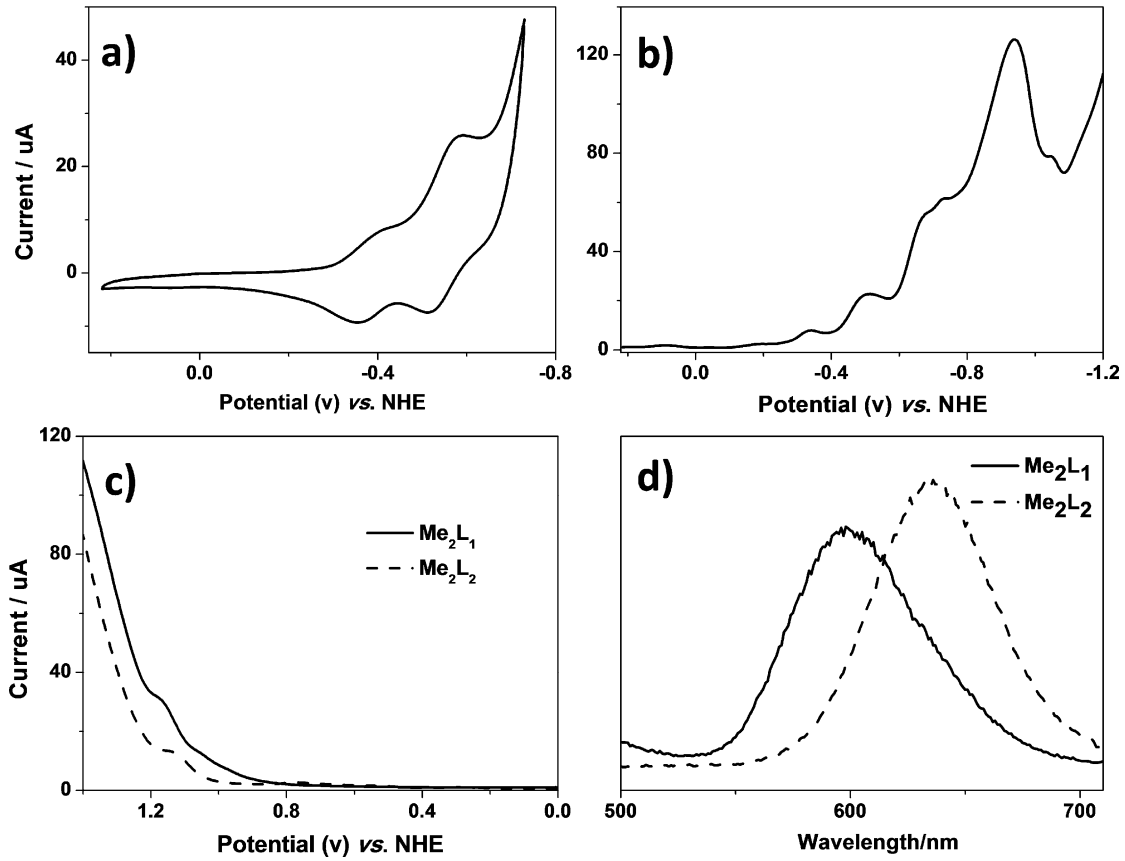

Figure 4. a) Cyclic voltammograms (CVs) of 0.2 mM Ni_4P_2 in a 2 M NaCl aqueous solution (pH 1.2). b,c) Differential pulse voltammetry (DPV) of 0.2 mM Ni_4P_2 (b) and 0.2 mM Me_2L_1 and Me_2L_2 (c) in a 2 M NaCl aqueous solution (pH 1.2) with a scan rate of 100 $mV s^{-1}$. d) Emission spectra of Me_2L_1 and Me_2L_2 in aqueous solution (pH 1.2) with 360 nm excitation for Me_2L_1 and 400 nm excitation for Me_2L_2.

a tunable platform for achieving synergistic functions from multiple components but also facilitate mechanistic studies of these processes.

Acknowledgements

We acknowledge funding from the U.S. National Science Foundation (DMR-1308229) and the National Natural Science Foundation of China (21471126 and 21422106). X.J.K. acknowledges the State Scholarship Fund from the China Scholarship Council (CSC). We thank K. Lu, X. Zhou, Y. Fu and C. Poon for experimental help and discussions.

Keywords: hydrogen evolution reaction · metal–organic frameworks · photocatalysis · polyoxometalate

How to cite: *Angew. Chem. Int. Ed.* **2016**, *55*, 6411–6416
Angew. Chem. **2016**, *128*, 6521–6526

[1] a) H. C. Zhou, J. R. Long, O. M. Yaghi, *Chem. Rev.* **2012**, *112*, 673–674; b) M. O'Keeffe, O. M. Yaghi, *Chem. Rev.* **2012**, *112*, 675–702; c) H. Wu, Q. Gong, D. H. Olson, J. Li, *Chem. Rev.* **2012**, *112*, 836–868; d) C. Wang, T. Zhang, W. Lin, *Chem. Rev.* **2012**, *112*, 1084–1104.

[2] a) J. Della Rocca, D. M. Liu, W. B. Lin, *Acc. Chem. Res.* **2011**, *44*, 957–968; b) M. P. Suh, H. J. Park, T. K. Prasad, D.-W. Lim, *Chem. Rev.* **2012**, *112*, 782–835; c) J. P. Zhang, Y. B. Zhang, J. B. Lin, X. M. Chen, *Chem. Rev.* **2012**, *112*, 1001–1033; d) B. Chen, C. Liang, J. Yang, D. S. Contreras, Y. L. Clancy, E. B. Lobkovsky, O. M. Yaghi, S. Dai, *Angew. Chem. Int. Ed.* **2006**, *45*, 1390–1393; *Angew. Chem.* **2006**, *118*, 1418–1421.

[3] a) L. J. Murray, M. Dincă, J. R. Long, *Chem. Soc. Rev.* **2009**, *38*, 1294–1314; b) Z. Guo, H. Wu, G. Srinivas, Y. Zhou, S. Xiang, Z. Chen, Y. Yang, W. Zhou, M. OKeeffe, B. Chen, *Angew. Chem. Int. Ed.* **2011**, *50*, 3178–3181; *Angew. Chem.* **2011**, *123*, 3236–3239.

[4] a) A. Dhakshinamoorthy, H. Garcia, *Chem. Soc. Rev.* **2014**, *43*, 5750–5765; b) M. Yoon, R. Srirambalaji, K. Kim, *Chem. Rev.* **2012**, *112*, 1196–1231; c) M. Zhao, S. Ou, C. D. Wu, *Acc. Chem. Res.* **2014**, *47*, 1199–1207; d) G. Q. Kong, S. Ou, C. Zou, C. D. Wu, *J. Am. Chem. Soc.* **2012**, *134*, 19851–19857.

[5] a) L. Ma, C. Abney, W. Lin, *Chem. Soc. Rev.* **2009**, *38*, 1248–1256; b) C. Wang, D. Liu, W. Lin, *J. Am. Chem. Soc.* **2013**, *135*, 13222–13234; c) C. Y. Lee, O. K. Farha, B. J. Hong, A. A. Sarjeant, S. T. Nguyen, J. T. Hupp, *J. Am. Chem. Soc.* **2011**, *133*, 15858–15861.

[6] a) A. Aijaz, A. Karkamkar, Y. J. Choi, N. Tsumori, E. Rönnebro, T. Autrey, H. Shioyama, Q. Xu, *J. Am. Chem. Soc.* **2012**, *134*, 13926–13929; b) G. Lu, S. Li, Z. Guo, O. K. Farha, B. G. Hauser, X. Qi, Y. Wang, X. Wang, S. Han, X. Liu, J. S. DuChene, H. Zhang, Q. Zhang, X. Chen, J. Ma, S. C. J. Loo, W. D. Wei, Y. Yang, J. T. Hupp, F. Huo, *Nat. Chem.* **2012**, *4*, 310–316.

[7] a) A. Dhakshinamoorthy, H. Garcia, *Chem. Soc. Rev.* **2012**, *41*, 5262–5284; b) W. W. Zhan, Q. Kuang, J. Z. Zhou, X. J. Kong, Z. X. Xie, L. S. Zheng, *J. Am. Chem. Soc.* **2013**, *135*, 1926–1933.

[8] a) X. Chen, S. Shen, L. Guo, S. S. Mao, *Chem. Rev.* **2010**, *110*, 6503 – 6570; b) X. Wang, K. Maeda, A. Thomas, K. Takanable, G. Xin, J. M. Carlsson, K. Domen, M. Antonietti, *Nat. Mater.* **2009**, *8*, 76 – 80; c) Z. Yu, F. Li, L. C. Sun, *Energy Environ. Sci.* **2015**, *8*, 760 – 775; d) M. Wang, K. Han, S. Zhang, L. C. Sun, *Coord. Chem. Rev.* **2015**, *287*, 1 – 14.

[9] a) W. M. Singh, T. Baine, S. Kudo, S. Tian, X. A. N. Ma, H. Zhou, N. J. DeYonker, T. C. Pham, J. C. Bollinger, D. L. Baker, B. Yan, C. E. Webster, X. Zhao, *Angew. Chem. Int. Ed.* **2012**, *51*, 5941 – 5944; *Angew. Chem.* **2012**, *124*, 6043 – 6046; b) F. Lakadamyali, M. Kato, N. M. Muresan, E. Reisner, *Angew. Chem. Int. Ed.* **2012**, *51*, 9381 – 9384; *Angew. Chem.* **2012**, *124*, 9515 – 9518; c) B. F. DiSalle, S. Bernhard, *J. Am. Chem. Soc.* **2011**, *133*, 11819 – 11821; d) S. Metz, S. Bernhard, *Chem. Commun.* **2010**, *46*, 7551 – 7553.

[10] a) H. Kind, H. Yan, B. Messer, M. Law, P. Yang, *Adv. Mater.* **2002**, *14*, 158 – 160; b) W. Hou, S. B. Cronin, *Adv. Funct. Mater.* **2013**, *23*, 1612 – 1619.

[11] a) T. Zhang, W. Lin, *Chem. Soc. Rev.* **2014**, *43*, 5982 – 5993; b) J. H. Cavka, S. Jakobsen, U. Olsbye, N. Guillou, C. Lamberti, S. Bordiga, K. P. Lillerud, *J. Am. Chem. Soc.* **2008**, *130*, 13850 – 13851; c) Y. Kataoka, K. Sato, Y. Miyazaki, K. Masuda, H. Tanaka, S. Naito, W. Mori, *Energy Environ. Sci.* **2009**, *2*, 397 – 400.

[12] a) S. Pullen, H. Fei, A. Orthaber, S. M. Cohen, S. Ott, *J. Am. Chem. Soc.* **2013**, *135*, 16997 – 17003; b) A. Fateeva, P. A. Chater, C. P. Ireland, A. A. Tahir, Y. Z. Khimyak, P. V. Wiper, J. R. Darwent, M. J. Rosseinsky, *Angew. Chem. Int. Ed.* **2012**, *51*, 7440 – 7444; *Angew. Chem.* **2012**, *124*, 7558 – 7562.

[13] C. Wang, K. E. deKrafft, W. Lin, *J. Am. Chem. Soc.* **2012**, *134*, 7211 – 7214.

[14] a) B. Rausch, M. D. Symes, G. Chisholm, L. Cronin, *Science* **2014**, *345*, 1326 – 1330; b) J. S. Qin, D. Y. Du, W. Guan, X. J. Bo, Y. F. Li, L. P. Guo, Z. M. Su, Y. Y. Wang, Y. Q. Lan, H. C. Zhou, *J. Am. Chem. Soc.* **2015**, *137*, 7169 – 7177; c) B. Nohra, H. E. Moll, L. M. R. Albelo, P. Mialane, J. Marrot, C. Mellot-Draznieks, M. O'Keeffe, R. N. Biboum, J. Lemaire, B. Keita, L. Nadjo, A. Dolbecq, *J. Am. Chem. Soc.* **2011**, *133*, 13363 – 13374.

[15] Z. M. Zhang, T. Zhang, C. Wang, Z. Lin, L. S. Long, W. Lin, *J. Am. Chem. Soc.* **2015**, *137*, 3197 – 3200.

[16] a) R. Irie, X. Li, Y. Saito, *J. Mol. Catal.* **1983**, *18*, 263 – 265; b) I. Mena, M. A. Casado, V. Polo, P. García-Orduña, F. J. Lahoz, L. A. Oro, *Angew. Chem. Int. Ed.* **2012**, *51*, 8259 – 8263; *Angew. Chem.* **2012**, *124*, 8384 – 8388; c) H. N. Kagalwala, A. B. Maurer, I. N. Mills, S. Bernhard, *ChemCatChem* **2014**, *6*, 3018 – 3026; d) F. Guzman, S. S. C. Chuang, C. Yang, *Ind. Eng. Chem. Res.* **2013**, *52*, 61 – 65.

[17] a) H. Lv, W. Guo, K. Wu, Z. Chen, J. Bacsa, D. G. Musaev, Y. V. Geletii, S. M. Lauinger, T. Lian, C. L. Hill, *J. Am. Chem. Soc.* **2014**, *136*, 14015 – 14018; b) J. Song, Z. Luo, D. K. Britt, H. Furukawa, O. M. Yaghi, K. I. Hardcastle, C. L. Hill, *J. Am. Chem. Soc.* **2011**, *133*, 16839 – 16846; c) K. von Allmen, R. Moré, R. Müller, J. Soriano-López, A. Linden, G. R. Patzke, *ChemPlusChem* **2015**, *80*, 1389 – 1398.

[18] a) X. B. Han, Y. G. Li, Z. M. Zhang, H. Q. Tan, Y. Lu, E. B. Wang, *J. Am. Chem. Soc.* **2015**, *137*, 5486 – 5493; b) J. J. Stracke, R. G. Finke, *ACS Catal.* **2014**, *4*, 79 – 89; c) H. Lv, Y. V. Geletii, C. Zhao, J. W. Vickers, G. Zhu, Z. Luo, J. Song, T. Lian, D. G. Musaev, C. L. Hill, *Chem. Soc. Rev.* **2012**, *41*, 7572 – 7589.

[19] J. H. Cavka, S. Jakobsen, U. Olsbye, N. Guillou, C. Lamberti, S. Bordiga, K. P. Lillerud, *J. Am. Chem. Soc.* **2008**, *130*, 13850 – 13851.

[20] W. Wardencki, J. Orlita, J. Namieśnik, *Fresenius J. Anal. Chem.* **2001**, *369*, 661 – 665.

Received: January 14, 2016
Published online: April 20, 2016

